Journal of Chromatography A 1689 (2023) 463755

Contents lists available at ScienceDirect

Journal of Chromatography A

journal homepage: www.elsevier.com/locate/chroma

Computational framework for the techno-economic analysis of monoclonal antibody capture chromatography platforms

Juan J. Romero[a], Eleanor W. Jenkins[b], Joshua Osuofa[a], Scott M. Husson[a,*]

[a] Department of Chemical and Biomolecular Engineering, Clemson University, Clemson, SC 29634 USA
[b] School of Mathematical and Statistical Sciences, Clemson University, Clemson, SC 29634 USA

ARTICLE INFO

Article history:
Received 13 October 2022
Revised 22 December 2022
Accepted 23 December 2022
Available online 24 December 2022

Keywords:
Membrane chromatography
Multi-objective optimization
Simulation-based optimization
Single-use chromatography

ABSTRACT

We developed a computational framework that integrates commercial software components to perform customizable technoeconomic feasibility analyses. The use of multiple software packages overcomes the shortcomings of each to provide a detailed simulation that can be used for sensitivity analyses and optimizations. In this paper, the framework was used to evaluate the performance of monoclonal antibody capture processes. To this end, the simulation framework incorporated dynamic models for the affinity chromatography step that were validated with experimental breakthrough curves. The results were integrated with an Intelligen SuperPro Designer process simulation for the evaluation of key performance indicators of the operations. As proof of concept, the framework was used to perform a sensitivity analysis and optimization for a case study in which we sought to compare membrane and resin chromatography for disposable and reusable batch capture platforms. Two membranes and one resin were selected for the capture media, which yielded six process alternatives to compare. The objective functions were set to be cost of goods, process time, and buffer utilization. The results of the optimization of these process alternatives were a set of operating conditions that display tradeoffs between competing objectives. From this application exercise, we conclude that the framework can handle multiple variables and objectives, and it is adaptable to platforms with different chromatography media and operating modes. Additionally, the framework is capable of providing ad hoc analyses for decision making in a specific production context.

1. Introduction

Typically, biopharmaceuticals are manufactured in multiproduct facilities that share resources among different programs [1]. Thus, flexible production processes capable of responding to sudden increases in demand are indispensable. To select the process that provides the greatest flexibility, the techno-economic feasibility of different alternatives must be established before large investments are made in equipment and materials. Process Analytical Tools (PAT), such as mathematical models and computational simulation tools, can be used to analyze the impact of changes on the process prior to implementation [2]. The framework used for this analysis must quantify the possible benefits in terms that are relevant for the application. The models used to simulate the process must depict the physical behavior of the operation accurately and account for the impact of different variables. Finally, the framework needs to provide parameter values for optimal operation conditions to enable a comparison of design alternatives that maximize process performance. Given the multiple requirements for the technoeconomic study, there is no standalone software capable of delivering the desired results.

For the development of a computational framework that could be implemented effectively in scenarios relevant to the biopharmaceutical industry, we selected monoclonal antibody (mAb) production as the model process. mAbs are used to treat chronic and acute conditions including immunological disorders, cardiovascular diseases, many forms of cancer, and, recently, COVID-19 [3,4]. Improvements in the upstream process, like the development of new cell lines and the adoption of perfusion technologies, have yielded higher titers and shifted the capacity bottleneck and economic load towards the downstream process (DSP) [5]. In this setting, several techno-economic feasibility studies have been conducted for mAb production, usually to evaluate continuous DSP alternatives [6,7]. The capture chromatography step has been the focus of these studies. In an affinity chromatography operation, a dynamic model is necessary to simulate the physical phenomena involved. These models vary in their complexity and applicability to different systems [8–10]. A simulation featuring a dynamic model is capable of predicting capture performance as a function of oper-

* Corresponding author.
E-mail address: shusson@clemson.edu (S.M. Husson).

https://doi.org/10.1016/j.chroma.2022.463755
0021-9673/

ating conditions [11–14], allowing for optimization relative to these conditions. When the simulation involves economic factors, the frameworks frequently rely on production simulation software for the calculation of the key performance indicator (KPI) [15]. These economic analyses usually do not include a dynamic simulation; thus, operating conditions affecting chromatography performance are kept fixed [16–18]. In this regard, frameworks that incorporate both dynamic simulations and cost analyses are preferred because they are able to optimize economic indicators by changing process operating conditions [19].

Instead of using the framework to assess the well-studied benefits of continuous process platforms, in this study we explored membrane chromatography as an alternative to the traditional resin capture chromatography. Recent commercial products for membrane chromatography show possible benefits for mAb capture that make it attractive for commercial applications [20]. For example, Purilogics and Cytiva have demonstrated the advantages of membrane technology at short residence times over their resin-based process alternatives [21,22]. Despite small-scale applications being the current niche for membrane capture chromatography, manufacturers offer membrane modules intended for large-scale applications in other operations of the DSP. For instance, Sartorius offers ion-exchange membranes for use in commercial mAb polishing applications in the form of stackable cassettes, making it possible to customize the membrane volume according to the production size [23]. We expect membrane modules for commercial-scale capture applications to be widely available soon. The overarching question is whether the productivity benefits justify the replacement of the well-established resin-based capture chromatography platforms in industrial production scenarios. Some techno-economic studies have sought to answer this question [20,24]; however, new simulation tools are necessary to stay current with the latest membrane technologies and to allow more customization in the study. A higher level of detail and personalization allows for the simulation of realistic manufacturing scenarios, which yields results that are relevant for industrial applications.

In this work, we present a computational framework able to compare and simultaneously optimize membrane- and resin-based mAb capture platforms in disposable and reusable configurations. The framework incorporates dynamic models and economic analysis from simulation software. In the following sections, we present the theory behind the chromatographic adsorption models used in the dynamic simulation, the formulation of the optimization problem, and the definition of the KPIs. The applicability of the framework is demonstrated with a hypothetical case study featuring state-of-the-art stationary phases. Through this limited case study, we will show the robustness and flexibility of the framework to adapt to specific scenarios and processes, with the level of detail necessary to achieve relevant results for decision-making.

2. Theory

Column breakthrough curves were simulated using computational realizations of mathematical models for membrane and resin chromatography found in the literature [25,26]. These computed results were validated against experimental data. This section provides an overview of our simulation-based optimization framework, along with the KPIs used to develop the objective functions.

2.1. Dynamic modeling of the chromatography column

The capture process comprises a sequence of operations: loading, washing, elution, and regeneration. In this work, loading and washing are simulated as dynamic systems. We assume behavior for the elution and regeneration steps. In the loading step, product molecules (e.g., mAb) in the feed stream are captured by binding sites located on the surface of the stationary phase (membrane or resin). Eq. (1) describes the liquid phase material balance for this step. $\boldsymbol{J}$ is the rate of mass per unit of volume leaving the liquid phase, C is the concentration in the liquid phase, u is the velocity vector and ω is the porosity of the media. Danckwerts boundary conditions are used as shown in Eqs. (2) and (3) [10].

$$\omega\frac{\partial C}{\partial t}+J=-\nabla\cdot(uC)+\nabla\cdot(D\nabla C) \tag{1}$$

$$-(D\nabla C)\cdot n=u(C_{in}-C)\ at\ inflow \tag{2}$$

$$\nabla C\cdot n=0\ at\ outflow \tag{3}$$

Only longitudinal dispersion is considered, meaning the dispersion tensor **D** in Eq. (1) has a single component (D). This component is described using a high Peclet number approximation (Eq. (4)). The parameter alpha is used as a fitting parameter to match experimental breakthrough curves [25].

$$D=\alpha*v \tag{4}$$

Once the breakthrough curve is obtained, we can estimate the dynamic binding capacity (DBC) for any breakthrough percentage. Eq. 5 illustrates this calculation for a 10% breakthrough (DBC_{10}), where MV is the media volume, $V_{10\%}$ is the load volume corresponding to a breakthrough value of 10% of the feed concentration. C_{in} and C_{out} are the concentration of the streams entering and leaving the solid media.

$$DBC_{10}=\frac{\int_{V_{hold}}^{V_{10\%}}(C_{in}-C_{out})\,dV}{MV} \tag{5}$$

2.2. Resin chromatography model

In resin chromatography, the rate of adsorption onto the solid phase is controlled by two mass-transport diffusion steps: one from the bulk to the resin through the film surrounding the particle in the packed bed and another from the surface of the resin particle to the binding site through the pores. In this latter case, an additional mass balance is necessary to describe the liquid concentration within the pores. Resin chromatography also requires two distinct porosities: for the bed (ω_b) and for the particle (ω_p) [27]. The rate of mass entering the solid phase is described by the shrinking core model [26]. This model is defined by the existence of two types of binding sites, each with its own adsorption rate and mass balance. The total solid phase concentration is the sum of the concentration for the two types of sites. In this model, the behavior of the rate of change in the concentration in both sites is defined by an adsorption rate and a desorption rate. The adsorption rate is proportional to the pore concentration and to a difference in concentrations in the solid phase. The derivation of the resin equations is shown in S2-S8 of Supporting Information.

2.3. Membrane chromatography model

In membrane chromatography, the feed solution passes through the pores of the stationary phase where the binding sites are located. This feature makes advection the controlling mechanism in membrane chromatography [28]. In contrast, in resin-based chromatography, the feed solution largely flows through the interparticle void volume, and mAbs must diffuse into and through the pores of the resin media to reach binding sites. The result is that the DBC for membrane chromatography is insensitive to flow rate. This allows for shorter residence times (RT) and, consequently, faster processes [29]. The lack of long-range diffusion from the bulk to the binding sites means that there is no additional material balance for the pores, and the rate of material leaving the liquid phase is equal to the adsorption rate in the solid phase [25].

For membranes, film and pore diffusive resistance can be neglected and an instantaneous adsorption process can be assumed. In this case, the solid phase concentration is described by an equilibrium isotherm. Different isotherm models such as Langmuir, bi-Langmuir, steric hindrance, and spreading model can be used to describe the thermodynamic behavior of the system [30]. These models differ in their degrees of freedom and in the way that they account for different molecular interactions between the adsorber and protein, depending on factors such as ionic strength and pH [31]. In this work, the Langmuir model was chosen because of its simplicity and ability to fit experimental data accurately.

Usually, void volumes in membrane chromatography modules are larger than resin-packed columns. For example, in a Sartorius Sartobind-Q cassette, the membrane occupies 1.6 L of the total 4.5 L module inner volume [23]. At the beginning of the capture operation, these spaces are filled with equilibration buffer (C=0) that act as a diluent for the feed. To account for this effect, the void volume was modeled as a perfectly mixed, continuously stirred tank reactor (CSTR) located before the membrane [25]. The set of equations describing the membrane adsorption in this simulation is presented in S9-S13 of Supporting Information.

2.4. Wash step model

The wash step was modeled to account for adsorption that may occur when there is still product passing through the system. In the resin model, the adsorption rate becomes negative as C is set to 0. Nevertheless, the total mass transfer coefficient (k_{total}) is, generally, small due to the approximation of q equal to q_{max}. Thus, the model-derived mass of product eluted during the wash is negligible.

Unlike resins, the instantaneous adsorption model used for the membranes requires modifications for the washing process. In this case, the equilibrium condition implies that the concentration in the solid phase will be zero if the concentration in the liquid is set to zero, which would result in complete elution during the washing step. However, this behavior is not observed in practice, where desorption does not occur significantly unless there is a reduction in pH caused by the elution buffer. To account for this discrepancy, the adsorption rate was set to zero when the model predicted negative values. This is implemented in the finite element approximation of the differential equation by setting the adsorption rate to zero in each of the elements that constitute the membrane.

2.5. Key performance indicators

Table 1 introduces the KPIs that were used to explore the behavior of the simulation (through sensitivity analyses) and to define the objective functions for optimization. KPIs were selected based on their frequent use in the literature and their capacity to assess the efficient utilization of resources such as time, raw materials, and capture media volume. The analysis of the selected KPIs is meant to provide insight into the influence of variables and parameters on process performance.

3. Materials and methods

3.1. Experimental breakthrough data

Purexa™A Protein A affinity membrane (0.2 mL) was purchased from Purilogics (Greenville, SC). Hitrap Fibro™ PrismA membrane (Cat # 17549856, 0.4 mL) was purchased from Cytiva (Buckingshamshire, UK). Polyethersulfone (PES) Nalgene Rapid-Flow Top Filter (0.2 µm, Cat. # 595-4520) was purchased from Thermo Fisher Scientific (Waltham, MA). Lyophilized human immunoglobulin G (hIgG ≥ 95%) was purchased from Lee BioSolutions (Maryland Heights, MO). Trisodium citrate dihydrate (≥99%) was purchased from Alfa Aesar (Ward Hill, MA). Citric acid (>99%) and phosphate buffered saline (PBS) powder were purchased from Sigma-Aldrich (St. Louis, MO).

Loading buffer A1 (1x PBS pH 7.4) was prepared by dissolving 1 pack of PBS powder in 1 L of deionized water from a Milli-Q® Ultrapure purification system (Millipore Corp., Bedford, MA) and adjusting to pH 7.4 using HCl. Elution buffer E1 was prepared by adjusting 0.1M citric acid with 0.1M trisodium citrate until pH 3.0 was reached. Buffers were sonicated after preparation and subsequently filtered through a 0.2 µm PES filter. hIgG solutions were prepared at 5 g/L in loading buffer A1 and filtered through a 0.2 µm PES filter.

DBC measurements were performed using an AKTA Purifier 100 chromatography system (Cytiva). Manufacturer volume specifications were used to calculate flow rate (or residence time) for each membrane. The order of chromatographic operations was: equilibration, hIgG loading from a 150 mL superloop, washing, elution, and washing. Membranes were equilibrated using 20 mL of buffer A1 and loaded to at least 95% saturation with respect to the UV signal of hIgG solution. Wash volume, using buffer A1, was 5 mL; and elution volume, using buffer E1, was 5 mL. The effluent from each membrane column was monitored using a UV detector at 280 nm.

DBC measurements were made using Eq. 5, where C_{in} is the protein loading concentration, $V_{10\%}$ is the volume at 10% breakthrough relative to the absorbance of 5 g/L hIgG solution, V_{hold} is the system holdup volume measured with 2 wt% acetone in loading buffer A1, and MV is the manufacturer specified membrane volume.

MabSelect PrismA resin (Cytiva) was used as the reference for the resin-based chromatography. The experimental breakthrough data were obtained from the work by Sun et al.[14]. To fit the shrinking core parameters for this resin, we selected data corresponding to loading of a 2 g/L hIgG solution at residence times of 1, 2, and 3 min. (see Fig. 4 of Sun et al.[14]).

3.2. Dynamic model fitting and validation

Parameter values in the models were determined using optimization to minimize the sum of the squared residuals between the experimental data and the simulated model. For membranes, the mass transport equation, Eq. (1), was closed using relationships defined in Eqs. (4), (S9), and (S11). An approximate solution was generated by discretizing in space using streamline-upwinded Galerkin (SUPG) finite elements and backward Euler discretization in time [34]. The resulting system is solved using FreeFEM finite element software [35].

Eq. (S13) was used to model the concentration entering the membrane. The value of V_{CSTR} was measured experimentally to be 1.0 mL for both membrane columns. The membrane thickness was measured as 0.4 mm for Purexa-A and 0.7 mm for Fibro PrismA. The porosity for both membranes was assumed to be 80% [23]. The Langmuir parameters (q_{max} and K) and the dispersity coefficient (α) are the fitting parameters for each membrane. They were found by minimizing the sum of squared residuals between the model and the data up to 80% breakthrough. This maximum breakthrough was selected according to preliminary results in which we observed the limitations of the model to describe the behavior of the system at higher percentage breakthrough. One of the derivative-free optimization algorithm in MATLAB (i.e., fminsearch) was used to perform the optimization and obtain the fitting parameters [36]. Derivative-free algorithms require only values of the objective function, allowing us to use the finite element model as a black box [37].

Table 1
Definition of the KPIs used in this work and the rationale for its selection.

KPI	Definition	Rationale
Maximum breakthrough	Quotient of the highest concentration of product leaving the column and the feed concentration (C_{feed}) at any point during the loading and washing steps [32].	This KPI is used to assess the accuracy of the dynamic simulation. To this end, the maximum breakthrough must be in the range set by the model validation.
Yield	Quotient of the total mass of mAb recovered as product in the elution pool and the total mass of mAb loaded onto the column [26].	Yield is a key indicator of process efficiency. It quantifies mAb recovered as a product after all process operations. Since neither elution nor desorption during wash are simulated, a 5% product loss is assumed based on the DBC obtained from the capture and wash simulations.
Capacity utilization (CU)	Quotient of the DBC before elution and the model-derived equilibrium binding capacity (EBC) for C_{feed} [12].	This KPI is an indicator of efficiency in the use of media volume, which has repercussions in the consumables cost.
Buffer consumption	Total volume of buffer consumed defined mathematically using Eq. (6)$V_{buffer} = V_{media} \times \sum_i MV_i$ (6)MV_i is the volume of buffer (in terms of media volume) used in each of the i operations that constitute the capture purification process.	This KPI accounts for the buffer used in a single batch. In addition to being related to the buffer costs it also can be used to assess sustainability and the overall footprint of the operation.
Product concentration	mAb concentration in the stream leaving the column during elution.	High product concentration is related to reduced buffer utilization and low processing time in subsequent DSP operations.
Process time	Sum of loading time (t_{load}) and additional times (t_{add}) attributed to all other operations in the capture purification process defined by Eqs. (7) and (8). $t_{load} = \frac{V_{batch}}{F_{load}} = \frac{V_{batch} * RT}{V_{media}}$ (7) $t_{add} = V_{media} \times \sum_i \frac{MV_i}{F_i} = h_{media} \times \sum_i \frac{MV_i}{v_i}$ (8) F_i is the flowrate for process i, v_i is the average flow velocity for process i and h_{media} is the column height/membrane thickness.	This KPI represents the total time necessary for the processing of one batch. This is useful to calculate either the maximum output given a time constraint, or the time needed to process a determined number of batches.
COG	Quotient of operating costs of the capture purification process and the total mass of mAb in the elution pool [15].	This KPI is an intensified measurement of cost. It enables comparison of economic efficiency of processes with different scales of production and yields. In this work, only consumables and buffer were considered in the operating costs.
Productivity	Quotient of the total mass of mAb product and the multiplication product of membrane/resin volume and process time [33].	This KPI is a compound indicator that relates product yield to the use of time and media. It is useful to compare the production rate of processes with different scales.

For resins, an approximate solution to the system of partial differential equations (PDEs) was generated using one-dimensional flow in the vertical direction and discretizing using finite differences in space over the length of the column. The result is a set of first-order ordinary differential equations (ODEs) that were solved using MATLAB implementations of ODE variable time stepping algorithm Ode15s [38]. Again, least squares minimization with MATLAB fminsearch was used to fit the five parameters needed for the shrinking core model (K_a, k_{a1}, k_{a2}, k_m and q_{max}) [11] and α for Eq. (4). For all three of the chromatography media, parameters were fitted for each of three data sets with distinct residence times. A weighted average of these values was used as the parameter estimate for all curves.

3.3. Framework structure

The framework employs simulation-based optimization, which is defined using a feedback loop between an optimization algorithm and a process simulation tool. The optimization algorithm exchanges information with the simulator, selecting input parameters based on feedback provided through evaluation of the objective functions. In our work, the optimization was performed in MATLAB; the simulation was performed using SuperPro Designer for material, time, and economic calculations; and FreeFEM or MATLAB was used for transport modeling (Fig. 1). Communication was established using Object Linking and Embedding (OLE) technology, which relies on the Component Object Model (COM) architecture shared by all these software environments. After the dynamic simulation generates the breakthrough curve for loading and wash operations, the DBC is calculated by numerical integration per Eq. 5. In the case of membranes (FreeFEM), the DBC result is recorded in a text file and then read by MATLAB. (For resins the DBC result is already in this environment.) Then, the DBC is exported to an Excel file along with other information necessary for the process system simulation. Excel is used to collect, process, and exchange information between the optimization algorithm and the process simulation in SuperPro Designer using Visual Basic for Applications. Finally, the simulation outcomes are saved in the Excel file and read by the optimization algorithm running in MATLAB.

As the multiple simulation programs offer complementary features, combining them enables a more comprehensive process simulation than any single software. FreeFEM, in the case of membranes, and MATLAB, in the case of resins, solve the transport equations and provide the DBC at the operating conditions specified by the MATLAB optimization algorithm. In the case of SuperPro Designer, we used the built-in libraries and models to perform material balances and economic calculations used by the objective functions [39]. The objective function values were then used to generate new design points for consideration.

3.4. Case study

The objective of the case study was to assess the benefits of six process alternatives defined using three chromatography media on disposable and reusable platforms. The stationary phases considered were the Prism-A resin, and the Purilogics Purexa™-A and Cytiva Fibro PrismA membranes. The design variables were the volume of chromatography media (membrane or resin) and residence time.

Whereas a reusable platform regenerates the chromatography media and stores it for future batches, the media in a disposable platform (usually contained in pre-packed columns) is used for a batch and discarded. To be economically feasible, the disposable platforms must feature lower media volumes than the reusable platforms for the same batch volume to process. This is achieved by dividing the batch volume into fractions and loading them in multiple cycles. In this case study, the number of cycles is set to match the lifespan of the media, i.e., the maximum number of cycles the media can be used before losing its performance due

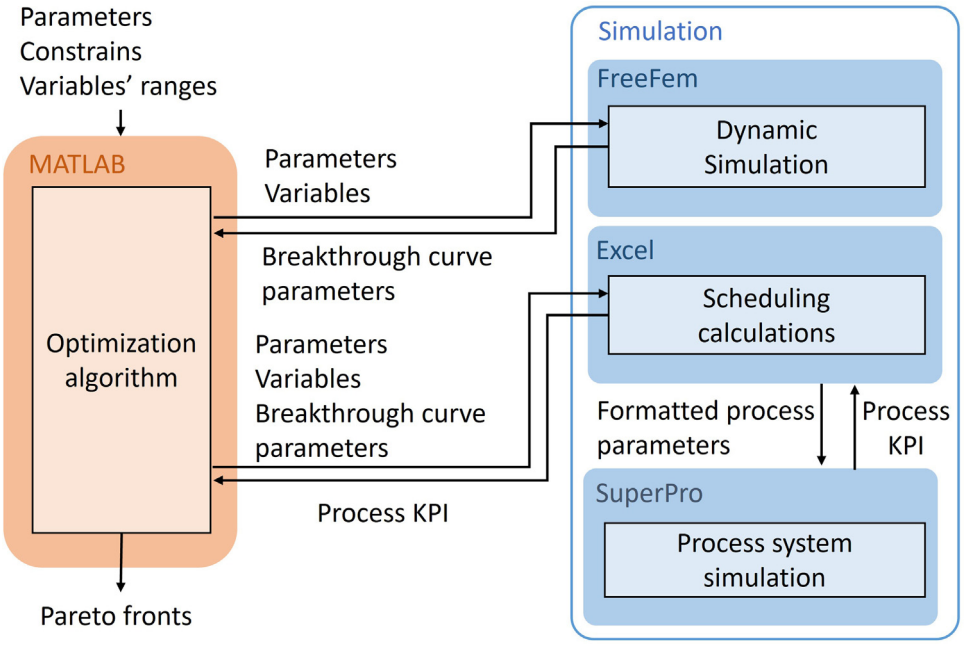

Fig. 1. General representation of the computational framework.

to fouling, Protein A leakage, and other deteriorating mechanisms. With this constraint, we ensured that the media is used until the end of its lifespan. Finally, the number of cycles was set to be one for the reusable platform since the media gets used until the end of its lifespan independently of the number of cycles per batch, and a single cycle offers the fastest operation.

We also designed the case study to evaluate the impact of the different process alternatives on resources that could act as constraints for the feasibility of the operation. For an existing facility, the constraints include the cost of the operation, process footprint, and allocated process time. Thus, we selected, optimized, and evaluated the tradeoff among three specific KPIs that represent the utilization of each of these resources. For cost, we selected COG as the indicator. Buffer consumption was selected as a KPI for process footprint because of the high impact that the buffer volumes have in the amount of waste produced in the operation. Finally, process time was selected as a KPI since it can be used to set shifts and ensure compliant holdup times.

3.5. Process simulation

The SuperPro Designer flowsheet consists of a chromatography column unit operated under bind and elute mode. A full cycle consists of load, wash, elution, and regeneration I operations. Additional regeneration II and equilibration operations are executed once per batch. Since the manufacturers of the membranes chosen in this study do not currently offer modules for large scale applications, the characteristics of such modules are estimated. The membrane to void volume ratio ($V_{membrane}/V_{cstr}$) was estimated using Sartorius Sartobind cassettes as a model (1.6 L membrane/2.9 L void space) [23]. There is no reference for these membranes in large-scale application, so we assumed a scenario where the cost per liter of membrane and the replacement frequency are the same as those of resins, which were retrieved from the SuperPro Designer library. A height of 15 cm was used for the resin column; this is an intermediate value in the recommended range for this parameter [40]. Fig. 2 displays the process flowsheet and Table 2 shows the process variables used as parameters for the processes in the case study.

Table 2
Fixed design variables.

Design Variables	Value
Ratio $V_{membrane}/V_{cstr}$	0.55
Buffer cost	$3/L
Stationary phase cost	$7358/L
MV Wash	10
v Wash	225 cm/h
MV Elution	4
v Elution	150 cm/h
MV Regeneration I	6
v Regeneration I	300 cm/h
MV Regeneration II	9
v Regeneration II	300 cm/h
MV Equilibration	6
v Equilibration	300 cm/h
V_{batch}	2000 L
Replacement frequency	80 Cycles

4. Results and discussion

4.1. Breakthrough curves, validation, fitting parameters

Fig. 3 shows the Purexa™-A and Fibro PrismA membrane breakthrough curves at different RT for experimental and simulated data. In the experimental data, there is no observable correlation between RT and the shape of the curves, which supports the equilibrium adsorption model as an appropriate choice. The model parameters were determined by fitting the model to the data for 5, 12 and 30 s RT and averaging the resulting values. These RT values were chosen because high productivity is expected for fast processes. Table 3 shows the averaged values used for the breakthrough simulation. Fig. 3 illustrates the good agreement between the empirical and simulated breakthrough curves up to 80% breakthrough. Above this value, steric hindrance effects begin to have a more significant effect on breakthrough [41] and the model loses some accuracy.

Similarly, for resin chromatography (Fig. 4), the parameter fitting was performed for each breakthrough curve and a weighted average was taken (Table 3). For the 1- and 2-min RTs, we observed an agreement between the simulated and experimental

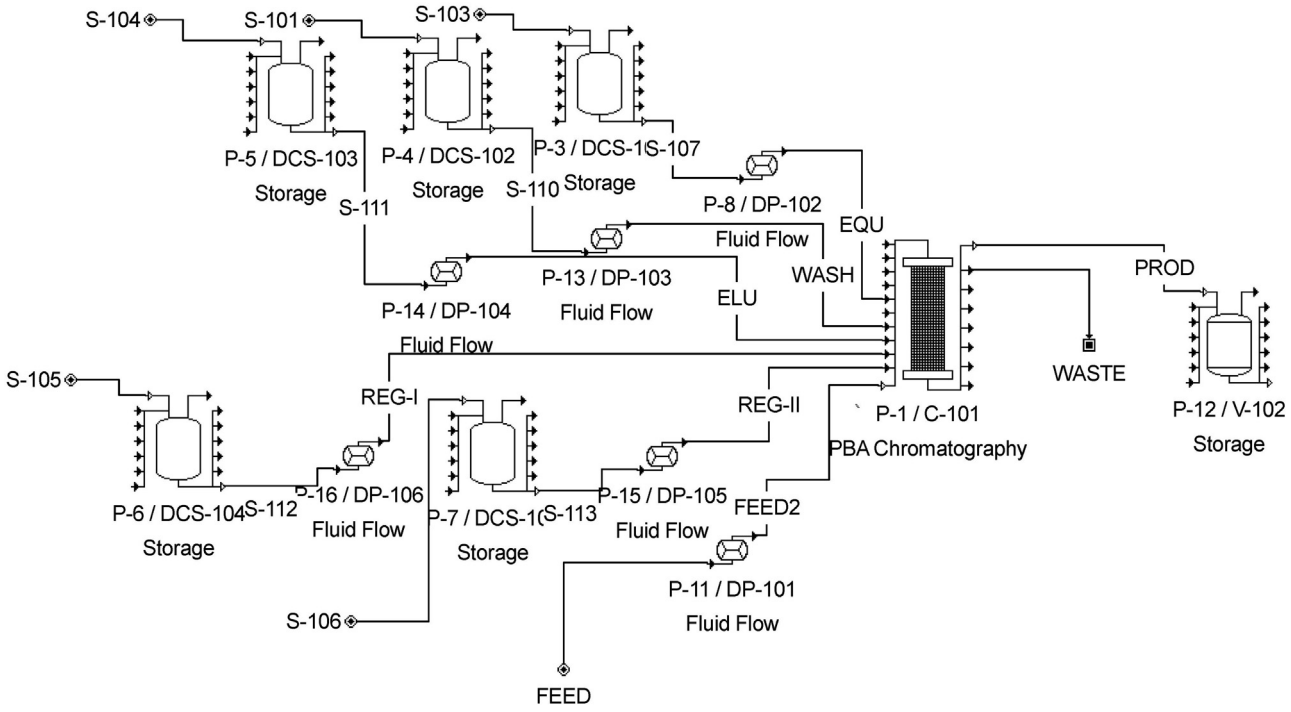

Fig. 2. Flowsheet for the capture process simulated in SuperPro Designer. The process solutions contained in Disposable Containers for Storage (DCS) are fed with Diaphragm Pumps (DP) into the chromatography unit (C). The resulting product is then recovered in a vessel (V).

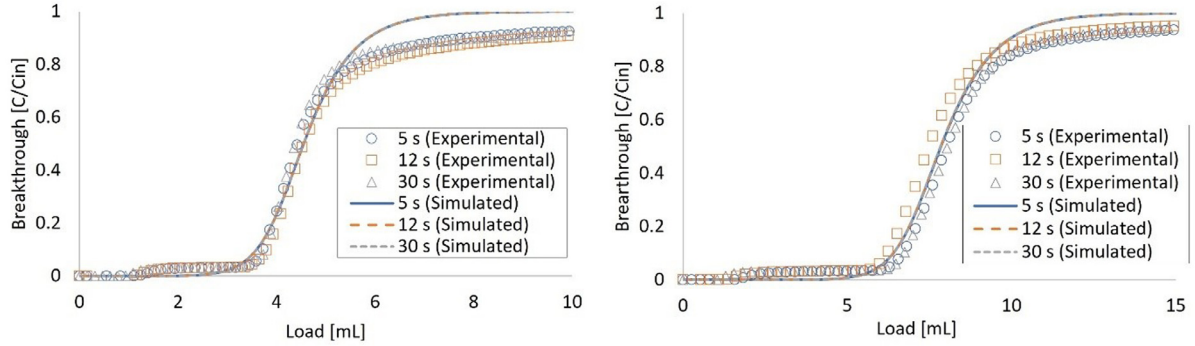

Fig. 3. Experimental and simulated breakthrough curves for Purexa™-A membrane (left) and Fibro PrismA membrane (right) at different RT. RMSE values for Purexa™-A membrane curves are 0.0283, 0.0370 and 0.0419 mL/mL for 5,12 and 30s RT. RMSE values for Fibro PrismA membrane curves are 0.0347, 0.0505 and 0.0401 mL/mL for 5,12 and 30s RT.

Table 3
Values for the fitting parameters

PrismA resin parameters					
K_a [L/g]	k_1 [g/(L min)]	k_2 [g/(L min)]	k_m [cm/min]	q_{max} [g/L]	α [cm]
101±23	0.377±0.137	0.199±0.046	0.00157±0.00166	139±11	0.0257±0.012
Fibro PrismA membrane parameters					
K [L/g]				qmax [g/L]	α [cm]
0.888±0.17				103±12	0.028±0.002
Purexa™-A membrane parameters					
K [L/g]				qmax [g/L]	α [cm]
0.623±0.207				117±10	0.0139±0.0005

breakthrough curves for values up to 90% breakthrough. For the 3 min RT, good agreement between simulation and experimental data is observed up to approximately 20% (0.4 mg/mL) breakthrough. Notably, the laboratory column has a height of 5 cm, so, to maintain the same average flow velocities for the commercial-scale process column (15 cm), the residence time interval must be adjusted from 1-3 min to 3-9 min.

4.2. Sensitivity analysis

The influence of the design variables on process KPIs was investigated by varying the media volume at two values of RT. Fig. 5 presents the results for reusable (single cycle) processes. The model-derived EBC values for the Prism-A resin, Purexa™-A membrane, and Fibro PrismA membrane were 87, 89, and 79 mg/mL.

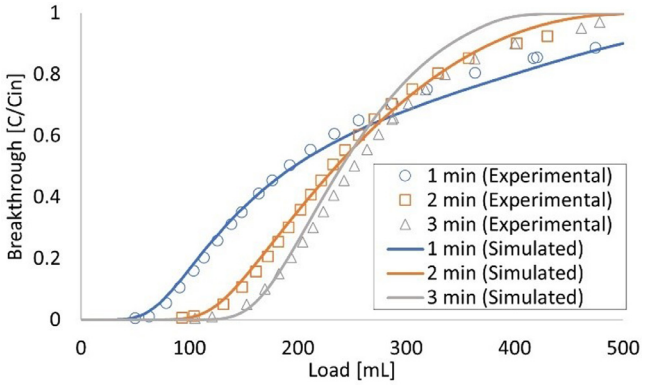

Fig. 4. Experimental [33] and simulated breakthrough curves for Prism-A resin at different residence times: 1 min (300 cm/h), 2 min (150 cm/h) and 3 min (100 cm/h). RMSE values are 0.0243, 0.0179 and 0.0557 mL/mL for 1, 2, and 3 min RT curves.

Fig. 5**A** shows maximum breakthrough attained after loading 2000 L batch feed with a 5 g/L titer. For all series, we have the same behavior; that is, almost 100% breakthrough at low media volumes and a gradual descent to 0% breakthrough when the media volume is large enough to capture all the loaded material. The difference in the shape of the curves is related to both the characteristic EBC of the media and the system dispersion. In our simulations, the curves for the resin chromatography columns present sharper fronts than the membrane columns at both levels of residence times. Additionally, the sharpness of the resin curve at higher residence times is consistent with a diffusion-controlled process.

In Fig. 5**B** we observe how yield is solely a function of media EBC at low media volumes, where the stationary phase is saturated, and breakthrough is close to 100%. However, as media volume increases, dispersion effects start to play a role in yield performance. In membranes, dispersion makes reaching 0% breakthrough difficult, provoking lower yields compared with resins at higher media volumes.

A different tendency for CU is observed in Fig. 5**C**. In the region of low media volume, where the media becomes saturated, CU is constant at 100%. CU starts to decrease as media volume increases. For large media volumes, amount of product per unit volume to capture is lower than for small media volumes because load is kept fixed. This reduction in relative load translates into low CU (underutilized media).

From the definition of buffer consumption (Eq. 6 in Table 1) we note this value is directly proportional to media volume. Since the relative buffer volumes (MV_i) are fixed parameters given by the capture protocol (Table 2), we observe a common line for all series in Fig. 5**D**.

The behavior of buffer consumption has an effect on the final product concentration (Fig. 5**E**) and yield. An increase in buffer consumption, specifically during elution, dilutes the product. This is more noticeable when the media is not saturated. We observe that at low volumes (complete saturation) the product concentration is controlled by yield performance. As volume increases, the rise in elution buffer consumption is compensated by higher yields. Nevertheless, as yield reaches its maximum value, the concentration becomes more dependent on media volume, and all series tend to converge.

The definition of process time (Eq. (7)) indicates that load time is inversely proportional to the media volume and proportional to RT. The additional time (Eq. 8)) is proportional to the media bed height, which is kept constant despite the changes in volume. This corresponds with Fig. 5**F,** where we see that the RT has a strong influence on process time. The result is that membrane processes are much faster than the resin processes, and the Purexa^{TM}-A membrane process is slightly faster than the Fibro PrismA one.

COG is affected by buffer consumption, yield, and media volume. The cost of the media as a consumable is proportional to its volume. In the same way, buffer cost is proportional to its utilization (which also is proportional to media volume). These costs can be decreased by lowering media volumes at the expense of yield. Yield affects COG through the cost of lost product and the total mass of product obtained in each batch. These competing factors lead to a minimum COG as shown in Fig. 5**G.** Figure S1 (Supporting Information) provides detail on this tendency and shows the minimum COG values and corresponding media volume for each process alternative.

In a similar way, productivity (Fig. 5**H**) reaches a maximum value with an intermediate value of media volume. This KPI offers a comprehensive measure of capture efficiency, as it considers how much product is obtained relative to the process time and media volume used. Initially, we observe a rise in productivity as increases in media volumes correspond with increases in process time and yield. This tendency continues until the point at which yield and process time stabilize. From this point on, any additional increase in media volume leads to a corresponding decrease in productivity. Figure S2 shows the maximum values for productivity and the corresponding media volumes.

For disposable platforms (Fig. 6), we observe the same KPI tendencies of the reusable single cycle platforms, but at a lower media volume scale. A volume scale from 0.5 to 2.6 L was selected for the sensitivity analysis to observe different maximum breakthroughs in the system. The minimum COG and maximum productivity are presented in Figures S3 and S4 with their corresponding media volumes.

The previous sensitivity analyses indicate that the flow rate influences only the time dependent KPIs (process time and productivity). In these cases, the performance increases with lower residence time, a behavior consistent with the instantaneous adsorption model used for membranes. Based on this, we set RT as a process parameter instead of a variable for membranes, fixing it at the lower bound of the search space (5 s).

The resin also exhibits higher performance in time dependent indicators at low RT. Unlike membranes, however, RT affects maximum breakthrough, along with other indicators conditioned by it (yield, CU, product concentration, annual processing time, COG, and productivity). We observe that all these KPI deteriorate at lower RTs. Thus, we select the design variables for resin processes to be both RT and column volume.

From the sensitivity analysis, we note the behavior of the KPIs as follows: maximum breakthrough defines the behavior of yield and CU; buffer utilization is directly proportional to the media volume; and process time is a function of media volume, RT, and column height/membrane thickness. The behavior of all other KPIs is explained by the interaction of yield, CU, buffer utilization, and process time.

When comparing disposable against reusable single cycle processes, we observe that the performance of most KPIs is comparable. This is the case with maximum breakthrough, yield, CU, and product concentration. In contrast, time-dependent KPIs, namely process time and productivity, are affected proportionally by the reduction in media volume. In the case of buffer consumption, we observe that the proportional reduction in media volume is compensated by a proportional increase in the number of cycles. This situation causes the wash, elution, and regeneration I buffer volumes to be the same as for single cycle platforms. Nevertheless, equilibration and regeneration II are operations that take place only once per batch. Thus, the lower media volume causes a reduction in the buffer utilization for these operations. This effect

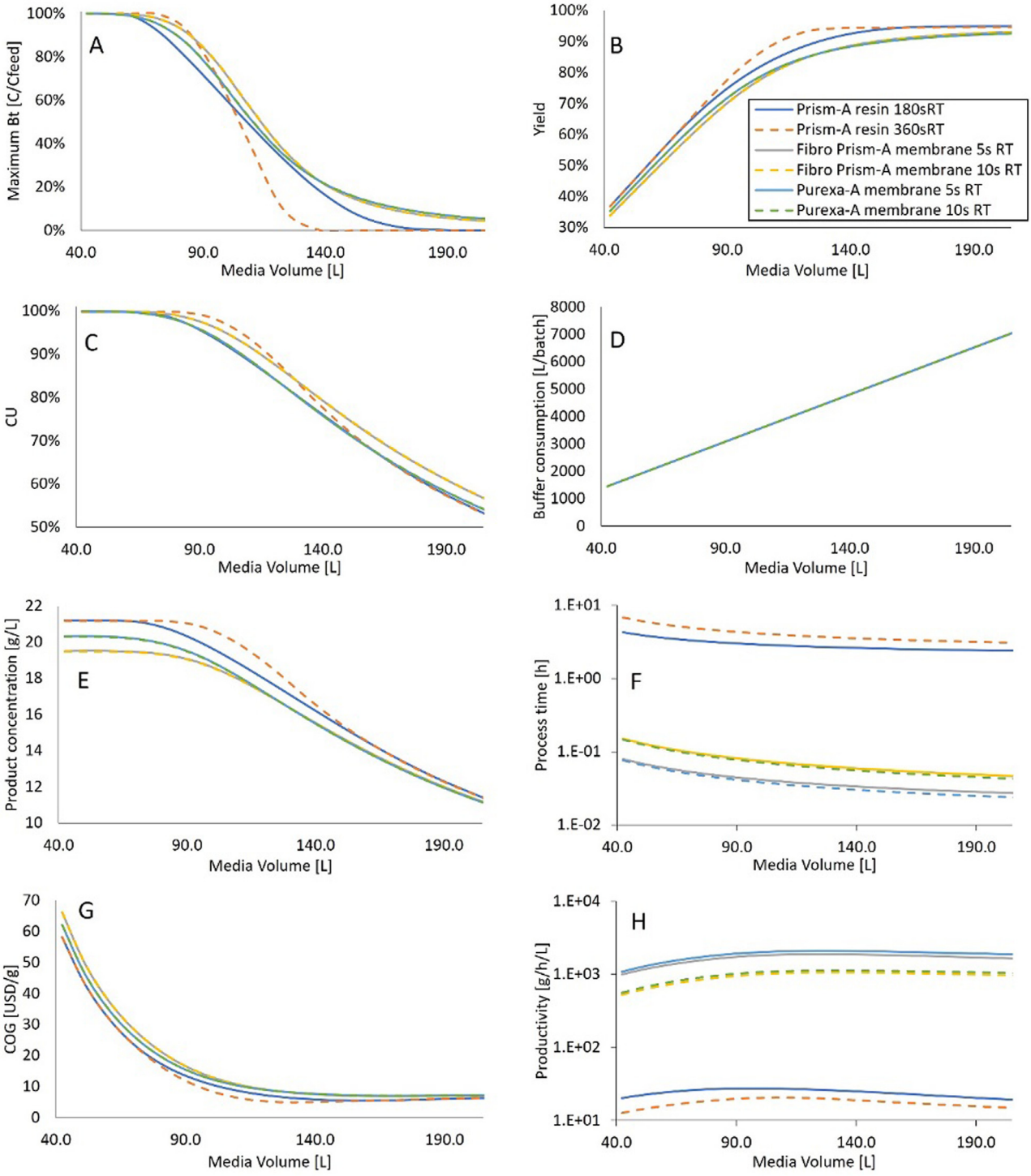

Fig. 5. Single cycle process sensitivity analyses for different KPI varying media volume for two values of residence time and three stationary phases. Fig. S1 (Supporting Information) provides detail on this tendency and shows the minimum COG values and corresponding media volume for each process alternative. Fig. S2 shows the maximum values for productivity and the corresponding media volumes.

translates into a reduction in total buffer consumption for disposable platforms compared with the single cycle process. These tendencies can be better observed when looking at the Pareto fronts presented in the next section. We see that disposable platforms have significantly higher process times than single cycle platforms. In contrast, disposable platforms require lower buffer consumption and have a slightly lower COG.

4.3. KPI tradeoff and optimization

Pareto fronts were generated using the multi-objective genetic algorithm (GA) in MATLAB [42]. When a single objective (i.e., COG) was needed, other derivative-free algorithms could be used. For each of the six platforms, the optimization results for the GA were obtained using five generations each with 25 members. The GA

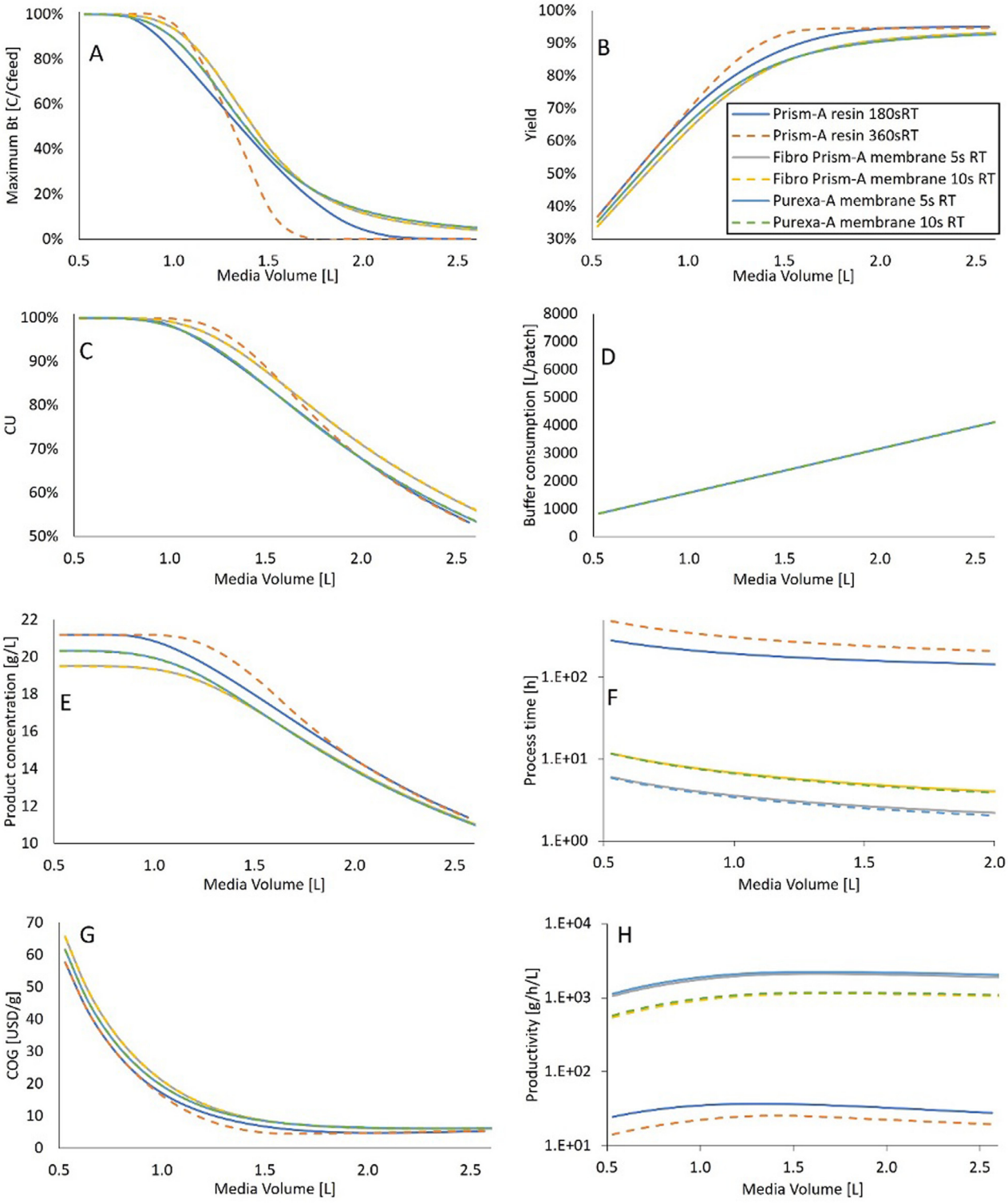

Fig. 6. Disposable media process sensitivity analyses for different KPI varying media volume for the different stationary phases. The minimum COG and maximum productivity are presented in Figs. S3 and S4 with their corresponding media volumes.

was set to optimize media volume for membrane-based platforms, and media volume and RT for resin-based platforms. Based on the sensitivity analysis, the search space was defined to be [40,200] L of media for the single cycle processes and [0.6-2.5] L for the disposable platforms. For the case of resin, a RT search space of [3-9] min was selected based on the range in which the model was fitted.

In the case of the Pareto fronts for buffer consumption and cycle time (Fig. 7), the optimal process configurations contain membrane volumes from the entire search space. This occurs because any improvement in cycle time is detrimental to buffer consumption, and vice-versa. This behavior can be observed in the sensitivity analisis (Figs. 5 and 6) where the buffer consumption increases steadly with increases in media volume. Meanwhile, pro-

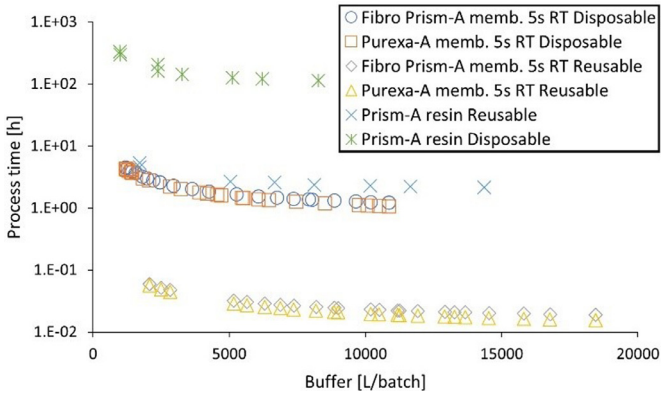

Fig. 7. Pareto fronts for process time and buffer utilization optimization for the different stationary phases in reusable single cycle and disposable configurations.

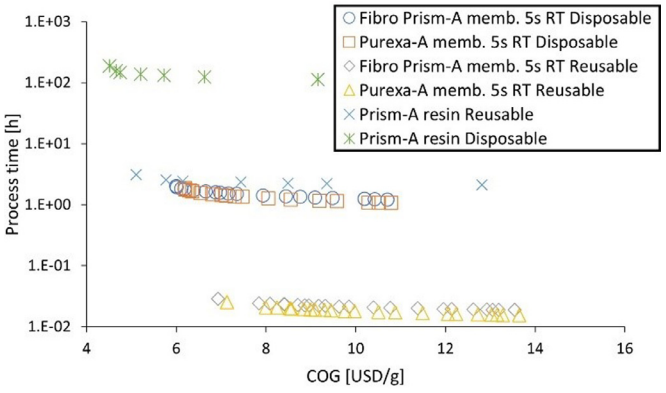

Fig. 8. Pareto fronts for process time and COG optimization for the different stationary phases in reusable single cycle and disposable configurations.

cess time decreases monotonically. Because of the much longer residence times in resin-based processes we observe a large difference in process time compared with membrane platforms.

In Fig. 8, the COG and process time points along the Pareto front represent membrane volume configurations spanning from a minimum value in COG (corresponding to around 180 L for single cycle platforms and 2.4 L for disposable platforms) to the top end of the search space. This behavior is consistent with the tendency of cycle time to decrease when media volume increases. Despite having RT as an additional variable, resins follow the same tendency with respect to volume, which is the main contributor to these KPI. We observe how resins can achieve lower COG than membranes due to the higher DBC, at the cost of high RT.

For the COG and buffer Pareto fronts (Fig. 9), the membrane volume spans from the value corresponding to the minimum COG towards the lower end of the search space (40L of media for the single cycle processes and 0.6L for the disposable platforms). This is consistent with the tendency of this indicator to decrease at low media volumes. As discussed in the sensitivity analysis, the buffer utilization constantly increases with media volume while COG reaches a minimum. Initially, as media volume increases, the accompanying yield decreases COG even as buffer consumption increases.

The final selection of the best process configuration will depend on the user's priorities and resources. However, it is possible to explore the process alternatives for our case study from the optimal operating conditions contained in the Pareto fronts. Comparing the membrane alternatives, the Purexa^{TM}-A offers a slightly shorter process time than the Fibro PrismA membrane. In contrast the Fibro PrismA membrane offers lower COG values due to its higher

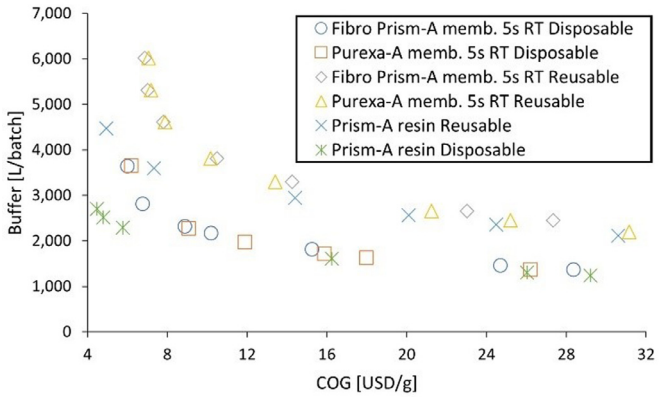

Fig. 9. Pareto fronts for buffer utilization and COG optimization for the different stationary phases in reusable single cycle and disposable configurations.

yield. At the moment, none of the membrane manufacturers offer modules suitable for large scale production processes, so the actual performance will depend on the void volume and the price of a real module.

Comparing the alternatives for single cycle operation, the resin-based process offers an advantage over membranes in terms of COG, as it reaches a minimum value that is 28-30% lower than the lowest values for the Fibro PrismA and Purexa^{TM}-A membranes. This comes with a high cost in terms of process time, which is 107 and 122 times longer than the Fibro PrismA and Purexa^{TM}-A. Despite the significantly longer process time, this value ranges from 2.1 to 3.1 h for all points in the Pareto front for the reusable resin platform, which is within a standard 8 h work shift. In the case of disposable processes, the membrane platforms are the only options able to attain process times suitable for one shift operation. While the process time for these platforms is in the range of 1.0-4.5 h, the resin based disposable process has a process time of 113-188 h. Finally, we can see how an increase in COG is the difference between a resin-based reusable platform and a membrane-based disposable platform, the latter of which is more efficient in terms of buffer consumption for the same range of process time. Finally, to compare all process alternatives we present the minimum KPI values observed in this study in Table 4. In this table, the optimal KPI values are normalized using the reusable resin platform as the base case.

4.4. Framework advantages and limitations

With a case study featuring both resin and membrane media, we demonstrated the ability of the framework to handle different types of media. However, the framework offers the option to evaluate addition media alternatives such as monoliths. If the media can be described using the previously presented models, then a change in parameters is the only requirement to adapt the framework. Otherwise, additional modifications may be needed, e.g., using a different isotherm equation to describe adsorption equilibrium. With these considerations, the framework could be used to simulate other affinity and non-affinity media used for capture or polishing operations.

The modular structure of the framework (see Fig. 1) offers the advantage of adjusting the level of detail of the simulation according to the user needs and knowledge of the operation. For example, if the parameters affecting breakthrough curves are kept fixed, the yield would be fixed as well, thus the dynamic simulation module could be eliminated. Moreover, other process simulation software with different features could be used instead of SuperPro Designer depending on the user's preference and resources—given

Table 4
Platform performance summary. Reusable Prism-A resin was selected as the base case.

Media	Operating condition	RT	Media Vol.	Normalized minimum		
				COG	Process t	Buffer Cons.
Prism-A resin	Reusable	[3-9] min	[40,200] L	1	1	1
Prism-A resin	Disposable	[3-9] min	[0.6-2.5] L	0.9	53.9	0.58
Fibro Prism-A memb.	Reusable	5 s	[40,200] L	1.4	0.01	1.00
Fibro Prism-A memb.	Disposable	5 s	[0.6-2.5] L	1.2	0.58	0.58
Purexa-A memb.	Reusable	5 s	[40,200] L	1.4	0.01	1.00
Purexa-A memb.	Disposable	5 s	[0.6-2.5] L	1.2	0.50	0.58

the software supports OLE technology). This structure allows the framework to simulate operations other than capture chromatography.

In the case study, we assess the capacity of the framework to yield optimized process conditions for different combinations of three KPI. Nevertheless, it is possible to select one or several of the eight KPI that the simulation provides as objective functions for the optimization problem. It also is possible to select different process parameters as variables. For example, instead of having media volume as a variable to find an optimal process time we could set media volume as a parameter and set flowrate as the variable to optimize productivity. This way, the new framework offers the advantage of customizing the optimization according to the problem characteristics.

Currently the framework has some limitations in optimization capacity and computational efficiency. It is capable of simulating only batch processes with continuous variables. In ongoing efforts, we are expanding its capacities to simulate multi-column continuous and semi-continuous platforms. The optimization algorithm for those platforms must handle mixed-integer values for variables like number of columns or cycles. The additional variables and more complex simulations are expected to have a considerable impact on the computational requirements for the optimization. Consequently, new strategies need to be implemented to improve the computational efficiency of the framework. Given that one of the objectives of this framework is the ease of implementation, the capacity to run on a general-purpose computer is essential.

5. Conclusions

A computational framework was developed for evaluating the performance of antibody capture processes. The proposed framework is robust and adaptable to specific products and platforms. The simulation elements of the framework are based on fundamental knowledge of the process, and its parameters can be obtained from experimental data. Results from the sensitivity analyses show how changes in process parameters impact the KPI in a consistent manner. This framework is flexible and capable of yielding customized information according to the user's needs. The KPI can be changed or modified according to the characteristics of a particular scenario and used to define objective functions for multiple or single objective optimization. The proposed approach of integrating different software proved to be effective in developing detailed simulations without requiring customized software development.

The applicability of the framework was demonstrated with a case study that aimed to assess the technoeconomic feasibility of a membrane-based processes in the context of large-scale production. In this study, six process alternatives were optimized and compared based on selected KPI (process time, COG, and buffer consumption). In the cases considered in this work, membrane platforms are attractive due to the short process time, though they present slightly higher COG than the resin platform in disposable and reusable configurations. This characteristic is essential in disposable platforms in which process times are considerably longer due to the multicycle operation. The disposable alternatives offer other benefits that are not investigated in this work. These benefits include the elimination of sanitization and cleaning steps, reduction of storage space utilization, reduced capital investment, amortization of the media cost, and reduction of the requirements for the production clean rooms. Based on the data of the case study, we believe membrane chromatography may be preferred in scenarios where disposable platforms are wanted and process time is a concern.

Declaration of Competing Interest

Scott Husson has an ongoing financial interest in Purilogics and provides consulting services to the Company.

CRediT authorship contribution statement

Juan J. Romero: Conceptualization, Formal analysis, Investigation, Methodology, Writing – original draft, Writing – review & editing. **Eleanor W. Jenkins:** Conceptualization, Formal analysis, Funding acquisition, Methodology, Resources, Supervision, Writing – review & editing. **Joshua Osuofa:** Investigation, Writing – original draft. **Scott M. Husson:** Conceptualization, Formal analysis, Funding acquisition, Methodology, Project administration, Supervision, Resources, Writing – review & editing.

Data availability

Data will be made available on request.

Acknowledgements

This work was supported by the National Institute of General Medical Sciences of the National Institutes of Health under award number R15 GM131341 and the National Science Foundation under award DMS-2011902. S.M.H. acknowledges support from the William B. "Bill" Sturgis, '57 and Martha Elizabeth "Martha Beth" Blackmon Sturgis Distinguished Professorship in Chemical and Biomolecular Engineering. We thank Dr. Dong-Qiang Lin's research group from Zhejiang University for kindly providing the breakthrough data for the Prism-A resin. Also, we thank James Angelo (Biologics Process Development, Bristol-Myers Squibb, Inc., Devens, MA) for helpful discussions concerning industrial capture processes.

Supplementary materials

Supplementary material associated with this article can be found, in the online version, at doi:10.1016/j.chroma.2022.463755.

References

[1] S. Misra, C.T. Maravelias, in: Overview of Scheduling Methods for Pharmaceutical Production, Springer, Cham, 2022, pp. 355–371, doi:10.1007/978-3-030-90924-6_13.

[2] FDAGuidance for Industry PAT - A Framework for Innovative Pharmaceutical Development, manufacturing, and Quality Assurance, 2004 http://www.fda.gov/cvm/guidance/published.html accessed August 4, 2020.

[3] I. Hernandez, S.W. Bott, A.S. Patel, C.G. Wolf, A.R. Hospodar, S. Sampathkumar, W.H. Shrank, Pricing of monoclonal antibody therapies: higher if used for cancer? Am. J. Manag. Care. 24 (2018) 109–112 www.ajmc.com. accessed April 5, 2021.

[4] P.C. Taylor, A.C. Adams, M.M. Hufford, I. de la Torre, K. Winthrop, R.L. Gottlieb, Neutralizing monoclonal antibodies for treatment of COVID-19, Nat. Rev. Immunol. (2021) 1–12, doi:10.1038/s41577-021-00542-x.

[5] J. Xu, X. Xu, C. Huang, J. Angelo, C.L. Oliveira, M. Xu, X. Xu, D. Temel, J. Ding, S. Ghose, M.C. Borys, Z.J. Li, Biomanufacturing evolution from conventional to intensified processes for productivity improvement: a case study, MAbs 12 (2020) 1770669, doi:10.1080/19420862.2020.1770669.

[6] V.K. Norbert Gottschlich, Purification of monoclonal antibodies by simulated moving-bed chromatography, J. Chromatogr. A. 765 (1997) 201–206, doi:10.1002/9780470444894.ch6.

[7] K. Behere, S. Yoon, Chromatography bioseparation technologies and in-silico modelings for continuous production of biotherapeutics, J. Chromatogr. A. 1627 (2020) 461376, doi:10.1016/j.chroma.2020.461376.

[8] L.K. Shekhawat, A.S. Rathore, Preparative biochemistry and biotechnology an overview of mechanistic modeling of liquid chromatography, Prep. Biochem. Biotechnol. 40 (2019) 623–638, doi:10.1080/10826068.2019.1615504.

[9] N.G. Pinto, E.E. Graham, Application of the shrinking-core model for predicting protein adsorption, React. Polym. Ion Exch. Sorbents. 5 (1987) 49–53, doi:10.1016/0167-6989(87)90164-4.

[10] S.Y. Suen, M.R. Etzel, A mathematical analysis of affinity membrane bioseparations, Chem. Eng. Sci. 47 (1992) 1355–1364, doi:10.1016/0009-2509(92)80281-G.

[11] D. Baur, J.M. Angelo, S. Chollangi, X. Xu, T. Müller-Späth, N. Zhang, S. Ghose, Z.J. Li, M. Morbidelli, Model assisted comparison of Protein A resins and multi-column chromatography for capture processes, J. Biotechnol. 285 (2018) 64–73, doi:10.1016/j.jbiotec.2018.08.014.

[12] D. Baur, M. Angarita, T. Müller-Späth, F. Steinebach, M. Morbidelli, Comparison of batch and continuous multi-column protein A capture processes by optimal design, Biotechnol. J. 11 (2016) 920–931, doi:10.1002/biot.201500481.

[13] J. Pollock, G. Bolton, J. Coffman, S.V. Ho, D.G. Bracewell, S.S. Farid, Optimising the design and operation of semi-continuous affinity chromatography for clinical and commercial manufacture, J. Chromatogr. A. 1284 (2013) 17–27, doi:10.1016/j.chroma.2013.01.082.

[14] Y.N. Sun, C. Shi, Q.L. Zhang, S.J. Yao, N.K.H. Slater, D.Q. Lin, Model-based process development and evaluation of twin-column continuous capture processes with Protein A affinity resin, J. Chromatogr. A. 1625 (2020) 461300, doi:10.1016/j.chroma.2020.461300.

[15] O. Yang, M. Qadan, M. Ierapetritou, Economic analysis of batch and continuous biopharmaceutical antibody production: a review, J. Pharm. Innov. 15 (2020) 182–200, doi:10.1007/s12247-018-09370-4.

[16] J. Pollock, J. Coffman, S.V. Ho, S.S. Farid, Integrated continuous bioprocessing: economic, operational, and environmental feasibility for clinical and commercial antibody manufacture, Biotechnol. Prog. 33 (2017) 854–866, doi:10.1002/btpr.2492.

[17] A.L. Grilo, M. Mateus, M.R. Aires-Barros, A.M. Azevedo, Monoclonal antibodies production platforms: an opportunity study of a non-protein-A chromatographic platform based on process economics, Biotechnol. J. 12 (2017) 1–10, doi:10.1002/biot.201700260.

[18] J. Hummel, M. Pagkaliwangan, X. Gjoka, T. Davidovits, R. Stock, T. Ransohoff, R. Gantier, M. Schofield, Modeling the downstream processing of monoclonal antibodies reveals cost advantages for continuous methods for a broad range of manufacturing scales, Biotechnol. J. 14 (2019), doi:10.1002/biot.201700665.

[19] B.K. Nfor, T. Ahamed, G.W.K. van Dedem, P.D.E.M. Verhaert, L.A.M. van der Wielen, M.H.M. Eppink, E.J.A.X. van de Sandt, M. Ottens, Model-based rational methodology for protein purification process synthesis, Chem. Eng. Sci. 89 (2013) 185–195, doi:10.1016/j.ces.2012.11.034.

[20] S. Nadar, G. Shooter, B. Somasundaram, E. Shave, K. Baker, L.H.L. Lua, Intensified downstream processing of monoclonal antibodies using membrane technology, Biotechnol. J. 16 (2021) 2000309, doi:10.1002/biot.202000309.

[21] Cytiva LifeSciencesHiTrap Fibro PrismA units HiScreen Fibro PrismA, 2021 https://cdn.cytivalifesciences.com/dmm3bwsv3/AssetStream.aspx?mediaformatid=10061&destinationid=10016&assetid=33339 accessed May 26, 2021.

[22] PurilogicsPurexa™ A - Protein A Membrane Chromatography for Fast Antibody Purification, 2021 https://www.purilogics.com/research-scale-affinity-membrane-adsorbers/purexa-a-protein-a-affinity-membrane-adsorber accessed September 21, 2021.

[23] Sartorius Stedim North America Inc.Sartobind® Cassettes, 4 and 8 mm Bed Height Product Datasheet, 2020.

[24] H. Varadaraju, S. Schneiderman, L. Zhang, H. Fong, T.J. Menkhaus, Process and economic evaluation for monoclonal antibody purification using a membrane-only process, Biotechnol. Prog. 27 (2011) 1297–1305, doi:10.1002/btpr.639.

[25] S. Dimartino, C. Boi, G.C. Sarti, A validated model for the simulation of protein purification through affinity membrane chromatography, J. Chromatogr. A. 1218 (2011) 1677–1690, doi:10.1016/j.chroma.2010.11.056.

[26] F. Steinebach, M. Angarita, D.J. Karst, T. Müller-Späth, M. Morbidelli, Model based adaptive control of a continuous capture process for monoclonal antibodies production, J. Chromatogr. A. 1444 (2016) 50–56, doi:10.1016/j.chroma.2016.03.014.

[27] E. von Lieres, J. Andersson, A fast and accurate solver for the general rate model of column liquid chromatography, Comput. Chem. Eng. 34 (2010) 1180–1191, doi:10.1016/j.compchemeng.2010.03.008.

[28] B.V. Bhut, S.M. Husson, Dramatic performance improvement of weak anion-exchange membranes for chromatographic bioseparations, J. Memb. Sci. 337 (2009) 215–223, doi:10.1016/j.memsci.2009.03.046.

[29] H. Trnovec, T. Doles, G. Hribar, N. Furlan, A. Podgornik, Characterization of membrane adsorbers used for impurity removal during the continuous purification of monoclonal antibodies, J. Chromatogr. A. 1609 (2020), doi:10.1016/j.chroma.2019.460518.

[30] P. van Beijeren, P. Kreis, T. Zeiner, Development of a generic process model for membrane adsorption, Comput. Chem. Eng. 53 (2013) 86–101, doi:10.1016/j.compchemeng.2013.03.005.

[31] B.K. Nfor, M. Noverraz, S. Chilamkurthi, P.D.E.M. Verhaert, L.A.M. van der Wielen, M. Ottens, High-throughput isotherm determination and thermodynamic modeling of protein adsorption on mixed mode adsorbents, J. Chromatogr. A. 1217 (2010) 6829–6850, doi:10.1016/j.chroma.2010.07.069.

[32] D. Baur, J. Angelo, S. Chollangi, T. Müller-Späth, X. Xu, S. Ghose, Z.J. Li, M. Morbidelli, Model-assisted process characterization and validation for a continuous two-column protein A capture process, Biotechnol. Bioeng. 116 (2019) 87–98, doi:10.1002/bit.26849.

[33] C. Shi, Z.Y. Gao, Q.L. Zhang, S.J. Yao, N.K.H. Slater, D.Q. Lin, Model-based process development of continuous chromatography for antibody capture: a case study with twin-column system, J. Chromatogr. A. 1619 (2020) 460936, doi:10.1016/j.chroma.2020.460936.

[34] A.B. Wilson, E.W. Jenkins, J. Wang, S.M. Husson, Numerical simulation of chemical separations using multimodal adsorption isotherms, Results Appl. Math. 7 (2020) 100122, doi:10.1016/j.rinam.2020.100122.

[35] F. Hecht, New development in freefem++, J. Numer. Math. 20 (2012) 251–266, doi:10.1515/JNUM-2012-0013.

[36] MathworksFind minimum of unconstrained multivariable function using derivative-free method - MATLAB fminsearch, 2022 https://www.mathworks.com/help/matlab/ref/fminsearch.html accessed January 11, 2022.

[37] J.C. Lagarias, J.A. Reeds, M.H. Wright, P.E. Wright, Convergence properties of the Nelder-Mead simplex method in low dimensions, SIAM J. Optim. 9 (1998) 112–147, doi:10.1137/S1052623496303470.

[38] L.F. Shampine, M.W. Reichelt, The MATLAB ode suite, 1997, doi:10.1137/S1064827594276424.

[39] I. IntelligenSuperPro Designer Product Features, 2020 https://www.intelligen.com/products/superpro-product-features/(accessed January 11, 2022.

[40] Global Life Sciences IP Holdco LLCSelection guide Packing HiScale, XK, and Tricorn chromatography columns with Capto and MabSelect resins 2, 2020.

[41] M. Nachman, Kinetic aspects of membrane-based chromatography immunoaffinity, J. Chromatogr. 597 (1992) 167–172.

[42] MathworksFind Pareto front of multiple fitness functions using genetic algorithm - MATLAB gamultiobj, 2021 https://www.mathworks.com/help/gads/gamultiobj.html accessed August 21, 2021.